

Palaeoseismology from microfabric and geochemical analysis of lacustrine sediment, Windermere, UK.

J. James Fielding¹, Alan E. S. Kemp¹, Jonathan M. Bull¹, Carol J. Cotterill², Richard B. Pearce¹, Rachael S. Avery¹, Peter G. Langdon³ & Ian W. Croudace¹

1 Ocean and Earth Science, University of Southampton, Southampton, National Oceanography Centre, SO14 3ZH, United Kingdom

2 British Geological Survey, Lyell Centre, Research Avenue South, Edinburgh, United Kingdom EH14 4AP

3 Geography and Environment, University of Southampton, University Road, Southampton, SO17 1BJ, United Kingdom

**corresponding author (jff1e13@soton.ac.uk)*

Abstract: Lake sediments commonly contain detrital layers that record events such as floods or earthquakes but these may be disturbed or partially destroyed by bioturbation. Here we use a novel combination of techniques to relate microscopic sediment fabric features to lake-basin scale processes. X-radiography and micro-XRF of cores are complemented by backscattered electron imagery and energy dispersive X-ray microanalysis of resin-embedded sediment. Together, the microfabric and geochemical methods enable the identification of clay-layer mass transport deposits despite bioturbational mixing of the original end members. Two cores with robust radionuclide chronologies contain correlative clay layers dated to 1979 (1974 – 1982) and 1979-1980 (1973 – 1986) respectively. These clay layers likely represent the distal turbidite generated by a major mass flow deposit identified from multibeam swath bathymetry and sediment grab sampling. A likely trigger for the mass flow and associated turbidity current is the 4.7 ML 1979 Carlisle earthquake. The lake basin slope was likely preconditioned for failure by increased sedimentary biogenic gas production and sediment in-wash as a result of anthropogenic activities, coupled with sediment disruption and dredging. This study highlights the effectiveness of microstratigraphic techniques in the recognition and characterisation of event layers in sediments where bioturbative disruption has occurred.

Keywords: microlithostratigraphy, palaeoseismology, palaeolimnology

Introduction

Lacustrine and marine sediments have the potential to serve as sensitive recorders of environmental changes and events driven by climatic, tectonic or anthropogenic processes. In particular, the deposits of lakes, or restricted basins such as fjords, commonly preserve high resolution records since sedimentation rates are comparatively higher than in the equivalent from open marine settings. In such cases, annual or even seasonal resolution may be attainable (Zolitschka et al. 2015; Schimmelfmann et al. 2016).

A major target in the analysis of the sedimentary records of lakes and marine margins has been to investigate the origins of slope-failures that produce scarps and generate mass transport deposits (MTD) and turbidites (Strasser et al. 2013; Schlolaut et al. 2014; Van Daele et al. 2015). Increasingly, such event deposits are being related to historical records of seismic activity and these efforts have led to the development of a new interdisciplinary field of “subaquatic palaeoseismology” that integrates marine and lacustrine sedimentology with palaeoseismology (Moernaut et al. 2009; Gracia et al. 2013; Strasser et al. 2013; Howarth et al. 2014; De Batist et al. 2017). Most of these sedimentary palaeoseismic records are being constructed in more seismically active regions (Moernaut et al. 2009; Howarth et al. 2014) and while historically based palaeoseismic records exist for Britain (British Geological Survey 2010; Stucchi et al. 2013), there are no such sedimentary palaeoseismic records. Critical evidence to associate sedimentary deposits with specific earthquakes includes synchronicity tests that require well-dated and clearly correlated sequences (Van Daele et al. 2015). Here we use a novel combination of techniques to study microscopic sediment fabric features in well-dated cores from Windermere to identify evidence for seismically generated MTD in sediments that have undergone disturbance by biota.

Many lacustrine sequences contain MTDs and turbidites with similar sedimentary and geochemical profiles from a range of sources including seismic and floods (Schlolaut et al. 2014). In order to interpret these features and build an accurate record of past extreme events careful analysis of the microfabric and structure of well-preserved sediments is sometimes necessary (Schlolaut et al. 2014). Ideally, this involves the analysis of annually laminated or varved records (Van Daele et al. 2014), but sediments in these settings are often subject to disturbance by biota even in environments with reduced water column turnover and resultant limited levels of bottom water oxygenation (Reynoldson 1987). Where sediments are disturbed by bioturbation the original structure may be obscured (McCall & Tevesz 1982). In particular, conventional optical microscopy of resin-embedded sediment may lack the necessary resolution to interpret microfabrics, for example Hage et al. (2017) found it difficult to distinguish burrows from fluid escape features using optical microscopy. To aid microfabric analysis we used Back Scattered Electron Imagery (BSEI) (Krinsley et al. 2005). BSEI is effectively an ultra-thin section image showing a porosity and composition signal in resin embedded sediment, and so is more informative than the optical image that contains optical “noise” from the entire thickness of the thin section. While BSEI has been extensively used in the study of varved sediments (Dean et al., 1999), studies of event deposits have primarily used optical microscopy for the highest resolution observations (Schlolaut et al. 2014; Hage et al. 2017). Our new approach may serve as an example for the future development of subaquatic palaeoseismology.

Study location and previous work

Windermere, in the Lake District of Cumbria, is England's largest natural lake being approximately 17 km in length with a maximum width of 1.5 km. Morphologically, the lake is divided into a 7 km-long North Basin with a maximum depth of 62 m and a 10 km-long South Basin with 44 m maximum depth (Fig. 1). These are separated by an extensive basement high that effectively creates the two depositionally distinct basins. Recent lake bed and subsurface studies have included single- and multi-channel Boomer profiles and 3D seismic reflection surveys (Vardy et al. 2010; Lowag et al. 2012; Pinson et al. 2013), as well as a detailed lake bed survey using multibeam swath bathymetry complemented by ROV bottom photography and sediment grab sampling (Miller et al. 2013). A series of piston cores recovered a late Pleistocene to Holocene sedimentary sequence whose overall stratigraphy is given in Avery et al. (2017). These investigations revealed evidence for several mass flow events characterised by scarps, transportation zones, and deposition zones (Miller et al. 2013). The largest and most recent of these is located on the distal shelf of the Trout Beck delta fan, extending 450 m into the lake to depths of 45 m (Fig. 2). The exact date and trigger mechanism for the Trout Beck mass flow event deposit have hitherto not been established.

Methods

Sediment sampling and sediment fabric analysis

Following the bathymetric survey, surface sediment grab sampling and piston, and gravity, coring reported in Miller et al. (2013), a further series of gravity cores were taken in 2014 with a Uwitec 86 mm diameter gravity corer. These gravity cores recovered the water-sediment interface and up to 46 cm of sediment. Sodium polyacrylate was used to solidify the water and preserve the water-sediment interface. This study uses the best preserved gravity cores from four sites shown in Figs. 1, 3. In total for this study four cores were split at the British Ocean Sediment Core Facility (BOSCORF), then processed and sampled using standard methods for high-resolution sediment fabric analysis (Kemp et al. 1998; Dean et al. 1999; Kemp et al. 2001). Split cores were slab sampled continuously with overlapping sections. The 1 cm-thick slabs were digitally imaged using a Geotek™ MSCL-CIS and X-rayed using a Hewlett Packard Faxitron X-radiography cabinet at 35 kV_e for 10 seconds. Following subsampling, slabs underwent fluid-displacive resin embedding after which covered thin sections (CTS) for optical microscopy and polished thin sections (PTS) for backscatter electron imagery were prepared. PTS were imaged and analysed using a LEO 1450VP Scanning Electron Microscope (SEM). Using a combination of the photomosaic backscatter electron images (BSEI), higher magnification BSEI and optical thin section microscopy, sediment fabrics and mineral and organic components were documented. Owing to their proximity to the Troutbeck delta failure scarp, high resolution photographic data from a fifth gravity core (core 53), and a grab sample taken in a coring campaign of 2013 was also used (Figs. 1, 2).

Geochemical analysis

The core archive-half surface was analysed using an Itrax Energy Dispersive X-Ray Fluorescence (ED-XRF) core scanner (Croudace et al. 2006) with a scanning step size of 200 μm , and a scanning window of 22 mm – 0.002 mm (Croudace et al. 2006). Data points were excluded from the analysis where surface discontinuities caused the total number of counts to drop below 20,000 kcps. Data points with zero validity or a mean standard error of >5 were also excluded from analysis following recommended procedures. Elemental data (counts) was normalised by dividing it by total kilocounts per second (kcps) for each interval to account for changes in the core density and surface high between sample points and cores (Croudace et al. 2006).

In order to calibrate and complement the ED-XRF semi-quantitative analysis, continuous 1 cm thick homogenised bulk samples were analysed to produce fully quantitative results using a Philips Magix-Pro Sequential Wavelength Dispersive XRF Spectrometer (Almelo – Holland), fitted with a 4 kW rhodium anode x-ray tube.

To link the coarser scale XRF geochemical analysis, the PTS for selected intervals were analysed in the SEM by energy dispersive X-ray spectroscopy microanalysis (EDS) using an Oxford Instruments X-Act 10mm² area Silicon Drift Detector. In addition to the analysis of individual grains, elemental maps and line scans were generated. Chemical characterisation of mineralogy was aided by use of the AZtec Energy software, which was also used to create true line scan data points at intervals of 200 μm through MTDs from (EDS) elemental map data. For direct comparison with SEM EDS at key intervals, the relevant PTS were also analysed by ED-XRF. To validate the mineral component of the debris lamina a 0.6 x 1 x 1cm sample was taken from 5.5 and 6.1 cm in SC64 and analysed by XRD using a Panalitical X'Pert Pro diffractometer with a Cu tube. Samples were ground for 8 minutes with 25% corundum in a McCrone micronizer in 5 ml of propan-2-ol. Samples were run from 2-76° θ and were compared with the ICDD 2016 mineral database.

Chronology

Bulk samples were taken at regular 2 cm intervals and analysed for ²¹⁰Pb and ¹³⁷Cs. Initially every other sample was analysed. Following this coarse scale analysis, resampling was undertaken to increase resolution where activity was highest. For all cores ²¹⁰Pb and ¹³⁷Cs was measured by direct gamma spectrometry using a Canberra well-type HPGe gamma-ray spectrometer counting for 100,000 seconds and evaluating the 661 keV peaks of the spectra as outlined in Ritchie & McHenry (1990) and Croudace et al. (2012). Each activity was corrected for sample mass and volume. The ²¹⁰Pb method (Flynn 1968; Croudace et al. 2012), uses a double acid leaching and auto-deposition onto silver discs methodology to determine ²¹⁰Pb activities of the samples. The mean sedimentation rate (MSR) and subsequent age estimates reported below are generated from ²¹⁰Pb activity and validated using ¹³⁷Cs.

A chronology was generated from excess ^{210}Pb activity data by applying the 'constant flux: constant sedimentation' (CF:CS) model (Robbins 1978). The model generates a MSR that is extrapolated down core. Outliers in natural log (Ln) excess ^{210}Pb , for example those affected by redox processes at the water sediment interface, or that were deposited by mass transport events, were excluded from analysis. Values of zero ^{210}Pb activity were also excluded from the analysis. Age error was calculated by applying the CF:CS model to the upper and lower machine error ^{210}Pb values to produce MSRs which were extrapolated down core to give an upper and lower age depth error estimate. All ages stated in this paper are given in years A.D. and are the median probability ages followed by machine error in brackets. ^{137}Cs was used to estimate dates of peak atmospheric nuclear weapons testing (1963) and the Chernobyl nuclear reactor incident (1986) (Ritchie & McHenry 1990; Croudace et al. 2012).

Results

Overall short core stratigraphy

The overall lithostratigraphy for both the North and South Basin short cores shows a tripartite structure with a lower pale brown mud overlain by a dark, more organic carbon-rich mud, which is in turn succeeded by paler mud (Fig. 3). In SC68 the lower pale brown section is laminated with alternating allochthonous detrital material and pale Fe-rich or Fe- and Mn-rich laminae. The middle dark, organic-rich mud (Gytja) corresponds to the mid-twentieth century period of enhanced lake eutrophication (McGowan et al. 2012). The upper paler sediments also contain concentrated diatom laminae and are enriched in Mn and other redox sensitive metals. In both SC68 and SC64 there is a distinct pale clay-rich layer above the dark gyttja that is entirely absent from the South Basin cores (Fig. 3). The clay-rich layer is marked by elevated potassium (K) and Titanium (Ti) (Figs. 5a/b, 6).

Age Model

The excess ^{210}Pb activity in SC68 and SC64 showed good correlation over the whole sampling interval indicating a near linear sedimentation rate (Fig. 4 a/b) (Appleby 2001; Tylmann et al. 2016). Through the MTD in both cores the MSR was not applied as this was assumed to be instantaneous. The SC64 excess ^{210}Pb CF:CS model (Fig. 4a) gave an MSR of 1.4 mm yr^{-1} ($1.2 - 1.6 \text{ mm yr}^{-1}$). A ^{137}Cs peak of 0.3 Bq/g at 4.5 cm was attributed to the 1986 Chernobyl nuclear reactor incident. No clear peak in ^{137}Cs was observed down core. This gave a ^{137}Cs MSR of 1.6 mm yr^{-1} and validated the ^{210}Pb age depth model to within 3 years (Fig. 4a). The SC68 excess ^{210}Pb CF:CS model (Fig. 4b) gave an MSR of 2.8 mm yr^{-1} ($2.5 - 3.0 \text{ mm yr}^{-1}$). A ^{137}Cs peak of 0.25 Bq/g at 8 cm was attributed to the 1986 Chernobyl nuclear reactor incident. No clear peak in ^{137}Cs was observed in SC68 down core. This gave a linear sedimentation rate based on ^{137}Cs of 2.7 mm yr^{-1} and validated the ^{210}Pb age depth model to within 2 years (Fig. 4b). ^{137}Cs mobility down core has been observed in other studies (Baskaran et al. 2016) and can occur due to bioturbation, soft sediment mixing or dissolution and diffusion in pore waters (Klaminder et al. 2012). In areas that received high

levels of ^{137}Cs from the Chernobyl nuclear reactor incidents, downward diffusion has been shown to overwrite the 1963 peak bomb testing signal and the first appearance of ^{137}Cs in 1953 (Appleby et al. 1990; Appleby et al. 1991). Both a muted 1963 peak bomb testing ^{137}Cs profile and diffusion of ^{137}Cs to sediments below 1953 have been observed at Grasmere, in the Windermere North Basin catchment (Barker et al. 2005).

High R^2 values in for the linear regression of the Ln^{210}Pb show that sedimentation rates are likely to be continuous through this section of the core (Appleby et al. 1990), however some outlying data points were removed from the analysis (Fig. 4). In SC64 ^{210}Pb data taken at 5 cm was lower than expected when compared to the linear trend of the ^{210}Pb for the rest of the core. This was likely due to the entrainment of older clays with low or no ^{210}Pb as part of the MTD.

Micro-lithostratigraphy of the clay rich interval

In core SC64 (Fig. 5a – left) the sediment shows an abrupt change from grey (7.5 Y 4/1) organic-rich mud to the light orange (7.5 YR 8/6) clay rich sediments at 8 cm. There is a further colour change to light yellow (7.5 YR 8/5) at 7.1 cm. The upper boundary at 5.6 cm is irregular and is marked by another abrupt change to overlying brown (10 YR 4/4) organic muds. The x-radiograph (Fig. 5a) shows a clear two-part structure within the pale orange/yellow horizon visible in the core with a very dense upper layer (5.6 – 6.2 cm) and a more diffuse lower part with density decreasing downwards to 8 cm. The BSEI (Fig. 5a) shows the 0.5 cm dense layer in the X-radiograph to correspond to a 0.5 cm thick K rich layer, reflecting the local lithological component is high in (Holmes 1964). The BSEI also reveals an underlying paler zone that is relatively enriched in clay. Small-scale redistribution of sediment due to zoobenthos burrowing, as well as some palletisation, is also evident from the BSEI (Fig. 5a). The ED-XRF Ti and K increase sharply at 8 cm (K also shown in Fig. 3), corroborated by increased values also in WD-XRF (Fig. 5a). Ti and K from ED-XRF both remain elevated to 6.5 cm, peak at 6 cm then decrease to 5.5 cm where values decrease in variability and remain low (Figs. 3; 5a). In addition discrete samples taken for XRD analysis from the clay rich strata between 5.5 and 6.1 cm in SC64 show that the pale laminae has a high total clay content of 32.6% (Table 1). At 6 cm, Mn values increase abruptly to peak at 5.5 cm, the highest value in the core (Fig. 5a).

In core SC68 (Fig. 5b), there is a colour change from grey (7.5Y 4/1) organic-rich mud to light brownish grey or dull orange clay-rich sediments (7.5YR 7/2 – 7/3) at 11 cm, with a further change at 10.5 cm to light orange (7.5YR 8/6). At 8.6 cm the clay rich sediment upper boundary is marked by a colour change to dull yellow orange organic muds above (10YR 6/3) (Fig. 5b). The X-radiograph shows a broad higher density (paler) interval corresponding to the pale yellow colour in the core surface but with a marked denser (paler) layer from 10.2 cm to 9.6 cm. BSEI show backscatter and clay content increases significantly between 9.8 and 9.5 cm (Fig. 5b), and pelletisation and redistribution of the

clay-rich sediment indicates significant bioturbation of the interval (Fig. 5 d, e). Analysis of SEM imagery and Itrax K shows that clay content remains high to 9.2 cm then gradually decreases to a diatom-rich lamina at 8.5 cm (Fig. 5b). Pellets are between 50 – 300 μm in diameter, and exhibit lithology and density of sediments from above and below, indicating redistribution of sediments by bioturbation (Fig. 5 c, e). The pale interval in the core is marked by elevated ED-XRF K and Ti from 10.5 – 8.5 cm with a peak in both at 9.8 – 9.5 cm corresponding to the palest (densest in the BSEI) sediment. Mn values decrease and become less variable through the clay rich sediments reaching a low at 9.7 cm depth. ED line scan of PTS show similar results in K with a peak spanning the clay (Fig. 6).

In both cores in the North Basin, the combined evidence from sediment fabrics and geochemistry is consistent with deposition of a distinct clay horizon followed by some bioturbative redistribution of the clay and this is discussed in more detail below. Independent ^{210}Pb and ^{137}Cs derived age models suggest that the clay horizons from both cores were deposited at the same time, with the SC64 clay horizon (6.2 – 5.6 cm depth) dating to 1979 (1974 – 1982) and the SC68 clay horizon (9.5 - 9.25 cm depth) to 1979 – 1980 (1973 – 1986).

Discussion

Origin of the clay horizon

In both cores SC64 and SC68, the pale clay appears as a relatively broad, 2 cm-thick horizon that is marked by elevated K and Ti over a similar depth range (Figs. 3, 5). However, the X-radiography and BSEI provide evidence for a thinner clay-rich compositional end-member (arrowed in Fig. 5) which has evidently been redistributed by bioturbation. The BSEI microfabric analysis reveals clusters of pellets rich in detrital clay and fine silt throughout this broader 2 cm-thick interval (Fig. 6). These pellets are consistent with evidence for vertical redistribution of sediments through bioturbation and the likely candidates for this activity in lake waters deeper than 20 m would be tubificid oligochaetes or chironomid larvae (McCall & Tevesz, 1982). Tubificid oligochaetes are conveyor belt feeders and redistribute sediments vertically by burrowing, passing material through the digestive tract and depositing faecal pellets in mounds at the water sediment interface (McCall & Tevesz 1982; Dafoe et al. 2011). Redistribution of sediments normally takes place over small vertical distances (2 – 9 cm) and ‘blurs’ sediment structure as opposed to completely removing original structures (McCall & Tevesz 1982). Furthermore, selective feeding can often result in the deposition of faecal pellets rich in clay and silt both above (Davis 1974; Ciutat et al. 2006) and slightly below (due to sediment slumping into burrows) (Fisher et al. 1980) the source sediment. Apart from tubificid oligochaetes, chironomid larvae are the other important component of the benthos and they create tubes and similarly sized faecal pellets (100 – 300 μm diameter) typically within the top 2 cm (Frouz et al. 2004; Nogaro et al. 2008), but primarily redistributing material downwards within oxygenated sediments

(Olafsson 1992). As seen in SC68 and SC64 microfabric clay rich pellets appear both below and above the concentrated clay rich end member, and therefore supports the bioturbative reworking of an originally compositionally pure clay end member. Furthermore, the broader less clearly defined K profile for SC68 further supports this. However, at SC64 the redistribution of the clay is primarily downward. The difference between the dominant nature of sediment redistribution between the two sites is likely due to a difference in the dominant fauna responsible for redistribution. Chironomid larvae were dominant at SC64 with evidence of downward mixing to depths of about 1.5 cm. The deeper parts of the basin were prone to seasonal anoxia during peak eutrophication in the latter part of the 20th century (Pickering, 2001) and tubificid oligochaetes were observed in abundance in the profundal sediments of Windermere even in anoxic conditions (Reynoldson 1987). It is therefore likely that a combination of oligochaetes and chironomid larvae were active in the deep basin (SC68) while chironomid larvae dominated in the shallower zone (SC64). While both sites hosted benthic fauna, the overall low oxygen conditions which prevailed in the lake in the 20th century, especially during thermal stratification and at depth (Pickering & Sutcliffe 2001), would have prevented extensive bioturbation from occurring helping to partially preserve some of the original structure.

The geochemical profile of Ti and K (high lithic component) and microlithostratigraphy of the SC64 clay is consistent with erosion and re-deposition of the laminated pre-Holocene detrital clay (Avery et al. 2017), silt and/or organic-rich Holocene lake muds. The clay constitutes the finest material settling out of suspension after the mass flow event that generated a turbidity current that penetrated a large part of the North Basin of Windermere. The characteristic geochemical profile of Ti and K, and sediment microlithostratigraphy is comparable with typical examples of the finest grained section or “clay cap” commonly described from other lacustrine debrite – turbidite deposits (Girardclos et al. 2007; Howarth et al. 2012; Simonneau et al. 2013; Strasser et al. 2013; Van Daele et al. 2015). The peak in Mn above the clay layer in SC64 (Fig. 5a) also supports this event bed origin. In many lakes with oxygenated bottom waters redox driven focusing causes sediments at the water sediment interface to become enriched in solid phase Mn (Davison 1993). As has been identified in marine settings (Colley et al. 1984; Jarvis & Higgs 1987; Thomson et al. 1987), and under experimental conditions (Chaillou et al. 2007), burial of solid phase Mn by an MTD can inhibit oxygenation of the underlying sediment leading to the reduction of Mn into its mobile reduced Mn^{2+} ions and upwards migration in the pore waters. On reaching oxygenated sediments above the clay reduced Mn^{2+} would then be re-oxidised and precipitated as Mn oxyhydroxides forming a fossilised oxygen front in the sediment (Fig. 9 d) (Davison 1993). While this phenomena is well described in a marine setting its occurrence is poorly represented in freshwater lake environments. A similar peak is not seen in SC68 since the deeper part of the basin was likely anoxic at the time the MTD was deposited (Pickering & Sutcliffe 2001), causing Mn to diffuse into the water column (Davison 1993). The higher variability in Mn in core SC68 deeper than 25 cm is related to

annual scale bottom water redox variability prior to the more eutrophic, and thus more intensely dysoxic, mid-20th century.

As regards the source of the turbidite, the scarp of the Trout Beck mass flow deposit exposes both the Holocene organic muds and the distinctive late Pleistocene glacial laminated silt and clay facies (see Avery et al. (2017), for the overall stratigraphy) (Figs. 2c, d, 9) (Miller et al. 2013) allowing these sediments to be redistributed as part of the MTD.

Origins and timing of the Trout Beck debris flow and relation to clay

The absence of the pale clay horizon from the South Windermere basin suggests that it originated as an event deposit that affected the North basin only and a likely candidate for its origin is the Trout Beck debris flow (Fig. 2). Analysis of high resolution photography and BSEI from core 53 (taken from the Trout Beck delta collapse scarp: Figs. 1, 2 and 7) shows laminated glacial clay (Avery et al. 2017) ending with an erosional unconformity, followed by two organic matter, sand, silt and clay rich layers. These beds represent debris from the Trout Beck scarp wall failure, but unlike SC64 and SC68 there is no pale clay horizon. The absence of a clay cap is likely due to the shallow setting of core 53 near the origins of the slope failure since the main body of suspended sediment from which the clay settled would have been concentrated in the deeper parts of the basin below the zone of slope failure, as is commonly the case for such events (Van Daele et al., 2015).

The debris layers are followed by 9 cm of organic mud in core 53 (Fig. 7). Using the MSR for SC68 (2.8 mm yr⁻¹) and SC64 (1.4 mm yr⁻¹) places the slope failure between 1950 and 1981. The grab sample, also taken from within the lower scarp, shows laminated glacial clays (Avery et al. 2017) abruptly terminating and overlain by only 7 cm of poorly consolidated Holocene mud (Fig. 2), further demonstrating the recent occurrence of the slide. The size, relative position (1.7 km NNE of SC64, 3.2 km SE of SC68), and recent age of the mass movements (Figs. 2; 7) makes the Trout Beck scarp the most likely source of the MTD described in SC64 and SC68 which have been dated to 1979 (1978 – 1986) and 1979 – 1980 (1973 – 1986) respectively.

With the timing constrained, possible causes of the slope failure may be explored. Trigger mechanisms for slope failure in lacustrine settings include seismogenic activity; overloading of slopes due to rapid or increased sedimentation; flooding associated with catastrophic river discharge; lake level fluctuations; surface wave activity (Girardclos et al. 2007); terrestrial debris flow or rock fall from adjacent slopes (Schlölaut et al. 2014); and anthropogenic activity, such as dredging (Girardclos et al. 2007). Flow data from the river Leven shows that the period 1978 to 1982 is a phase with above average, but not exceptional, winter outflow (National River Flow Archive, CEH, NERC – Fig. 8). Sedimentological analysis shows that neither SC68 nor SC64 MTDs contain macro organic fragments or detrital sand and silt in amounts in excess of the average for Holocene muds. Furthermore, geochemical and microlithostratigraphic analyses show no evidence for a

contemporary event in the South Basin or for other peak flow events, such as the exceptional 2008 – 2009 floods. There is therefore no evidence to support flooding as a trigger. There is also no record of significant lake level fluctuations during this period as shown by river out flow data in Fig. 8. Terrestrial slope failure is also not documented at this time.

The 1979 Carlisle Earthquake

The UK is an area of low to moderate seismic activity; however, recurrence relationship analysis of historical records shows that 4.7 ML earthquakes occur on average every 10 years (Baptie et al. 2005; Musson & Sargeant 2007). On the 26th of December 1979 a 4.7 ML earthquake with an epicentre 13 km NNE of Carlisle, (70 km N of Windermere town) occurred. The earthquake was one of the largest in the UK in the last century and was followed by two aftershocks in early January 1980 each measuring 3.8 ML (King 1980; Musson & Henni 2002). The earthquake's effects were felt at VI EMS (European Macroseismic Scale) in Carlisle and above III EMS over an area of 84 000 km², although intensity decreased rapidly to the south of the epicentre. Over much of the Lake District, the intensity was IV EMS and data suggest that the intensity was III - IV EMS in the Windermere and Kendal area (Musson & Henni 2002). These intensities are lower than the minimum intensities interpreted as necessary to generate debris flows in several lakes worldwide, where these range from slightly lower than VI (Wilhelm et al. 2016) to between VI and VII (Monecke et al. 2004; Howarth et al. 2014; Moernaut et al. 2014; Van Daele et al. 2015; Wilhelm et al. 2016) although Moernaut et al. (2014) notes that slopes susceptible to failure, (e.g. delta fans) may fail at lower intensities. Furthermore, as shown by Girardclos et al. (2007) slope failure can occur spontaneously, and, the timing of the Carlisle earthquake and its aftershocks (1979-1980) together with the lack of another contemporaneous mechanism suggest that it was a likely trigger of the Trout Beck delta fan failure and resulting mass transport deposits.

The Carlisle earthquake is the most likely cause of the Trout Beck delta fan slope failure and the resulting North Basin MTD. Previous earthquakes with epicentres closer to Windermere, albeit with lower magnitudes, in 1901 (4.1 ML) and 1915 (4.0 ML) have, however, not left evidence on the same scale in the lake bed sediments since the clay layer is unique within these records (Fig. 3). Even small earthquakes may cause considerable disruption if the sediment is destabilised by processes such as rapid sediment accumulation or biogenic gas production, prior to the event (Nisbet & Piper 1998). For example, although the 1865 Barrow-in-Furness earthquake was probably only in the range 2.5 – 3.5 ML, it produced spectacular and damaging liquefaction enhanced by the presence of saturated tidal sands (Musson 1998).

Slope preconditioning and failure

Biogenic gas build up as a result of sedimentary methanogenesis has been shown to intensify with increased organic matter input in eutrophic lakes systems (Kelly & Chynoweth 1981). The MTD overlays an organic-rich diatomaceous sediment thought to represent peak eutrophic conditions in the lake. Lake monitoring and previous sediment studies have shown seasonal cultural eutrophication of Windermere has occurred since the 19th century (Sabater & Haworth 1995; McGowan et al. 2012). Increased lake productivity as a result of additional nutrient loading and organic matter in-wash, is therefore likely to have led to increased biogenic gas in the sediments and reduced slope stability. However, Windermere has only been seasonally eutrophic since the mid-19th century meaning excess biogenic gas production is likely to be restricted to at most the top 40 cm, reducing the impact of this as a slope failure trigger mechanism.

Increased sediment loading causes additional pore pressure further reducing slope stability (Wilhelm et al. 2016), especially in steep delta fan slopes (Girardclos et al. 2007). AMS radiocarbon age depth models from piston cores taken at corresponding sites to the gravity cores show that MSR have accelerated since the 19th century (pre-19th century MSR PC 68 = 3 mm yr⁻¹, PC 64 = 3 mm yr⁻¹) (Avery et al. 2017). The Trout Beck delta fan has a slope angle of up to 7°, and while the Trout Beck catchment is relatively small in comparison to the Rothay/Brathay catchment to the North, the high elevation over a short distance and trapping efficiency of an intermediary smaller lake in the Rothay/Brathay catchment means the Troutbeck catchment is sedimentologically more important (Miller et al. 2014). Thus, increased sediment loading may have contributed to slope destabilisation.

There is evidence of commercial dredging for sand and gravel in the lake particularly around the submerged Trout Beck delta fan leaving visible pot marks scar in the sediment which flank the slope failure (Fig. 2a). This activity ended in the early 1970s (Miller et al. 2013), and so while it was not likely to have led directly to the slope failure, it is entirely likely that this activity could have further destabilised the delta fan. It is therefore probable that a combination of biogenic gas production, increased sediment loading and anthropogenic activity such as dredging have led to a critical state where sediment failure may occur in the lead up to the 1979 Carlisle earthquake.

Likely event timeline

- Increased biogenic gas production as a result of increased productivity in the lake since the 19th century, combined with increased sediment loading and activities such as dredging cause the steep-sided (7°) Trout Beck debris fan to become unstable, possibly facilitated by a geotechnical weakness at the glacial clay – Holocene mud boundary (Strasser et al. 2013).

- On the 26th of December 1979 an earthquake with an epicentre north of Carlisle occurs with an intensity of III-IV EMS in the Windermere and Kendal area (King 1980), causing failure of the Trout Beck delta fan slope (Fig. 2).
- Debris is transported as far as 1.7 km from the slope failure and fine-grained sediments (Holocene muds and glacial clay and fine silt) are suspended in a turbidity current that penetrates throughout large parts of the North Windermere Basin (Fig. 9). Following this, the fine grained sediments settle out of suspension in order of density, covering the organic rich sediments of the North basin below the depth of the slope failure, with at least 3.5 mm of clay rich sediment up to 3.2 km away.
- The MTD restricts oxygenation of the underlying sediments causing reductive mobilisation of Mn followed by precipitation of oxyhydroxides on reaching oxygenated sediment above the MTD giving rise to a peak in Mn. In profundal sediments persistent anoxia prevents the formation of Mn oxides-oxyhydroxides (Fig. 9).
- The clay horizon is variably vertically redistributed by bioturbation (Fig. 5 e). Microfabric analysis using BSEI and EDS analysis shows pelleting of the sediments suggesting that it was the result of conveyor belt feeding by tubificid oligochaetes and/or chironomids (Fig. 5).

Conclusions

A combination of Scanning Electron Microscope (SEM) sediment microfabric and geochemical analyses are used to identify event layers in the sediments of Windermere. These constitute the first evidence of seismic activity-induced mass transport deposits (MTD) preserved in lake sediments in the UK. Our microlithostratigraphic approach facilitated the identification of a MTD in two sediment cores (SC68, SC64) collected from Windermere's North Basin in 2014. Using a ^{210}Pb CF:CS age model, validated by ^{137}Cs profiles both MTDs were dated simultaneously to 1979 (1978 – 1986) and 1979 – 1980 (1973 – 1986).

Microfabric analysis using light and backscatter electron microscopy, and energy-dispersive X-ray microanalysis shows that the redistribution of sediments in faecal pellets through conveyor belt feeding by infaunal burrowers, has led to 'blurring' of the fine scale structure of the MTDs, especially in the more profundal SC68. Despite the redistribution of the original MTD clay, microstratigraphic techniques permit the identification of the initial MTD structure and accurate dating of the event. These results demonstrate that even if sediments are pelletised, event beds may nevertheless be detected using appropriate SEM microfabric and geochemical methods. The microlithostratigraphic analysis shows that the MTDs consist of reworked Holocene organic mud and Pleistocene age glacial detrital clays. SC64 has a classic 'debrite – turbidite clay cap' profile and shows K distributions comparable with other examples of MTDs found in lacustrine.

The MTD origins are linked to a large recent subaqueous slope failure of the Trout Beck delta fan, and associated mass flow deposit that was identified by previous investigations. Exploration of historic records reveals the most likely cause of the Trout Beck mass flow event and subsequent North Basin MTD to be an 4.7 ML earthquake on the 26th of December 1979 with an epicentre 70 km North of Windermere. It is likely that recent increased biogenic gas production, sedimentation, and commercial dredging combined to destabilise sediments in the Trout Beck area effectively preconditioning the sediment to a critical state.

Funding: This research was supported by a University of Southampton Studentship Grant and a Natural Environmental Research Council Studentship Grant (NE/L50161X/1) and the BGS University Funding Initiative (Reference S243).

Acknowledgements: We thank the British Ocean Sediment Core Research Facility for use of facilities and support. C. Cotterill publishes with permission of the Executive Director of the British Geological Survey, Natural Environment Research Council. We are very grateful to Karel Schulmann and two reviewers for their helpful comments, which greatly improved this manuscript. We would also like to thank the University of Southampton thin section workshop, GAU-Radioanalytical dating laboratories, Ross William and BOSCORF.

References

Appleby, P., Richardson, N. & Nolan, P. 1991. ²⁴¹Am dating of lake sediments. *Hydrobiologia*, **214**, 35-42.

Appleby, P., Richardson, N., Nolan, P. & Oldfield, F. 1990. Radiometric dating of the United Kingdom SWAP sites. *Philosophical Transactions of the Royal Society of London B: Biological Sciences*, **327**, 233-238.

Appleby, P.G. 2001. Chronostratigraphic techniques in recent sediments. In: Last, W.M. & Smol, J.P. (eds) *Tracking environmental change using lake sediments, volume 1: basin analysis, coring, and chronological techniques*. Kluwer Academic, Dordrecht, 171-203.

Avery, R.S., Xuan, C., Kemp, A.E., Bull, J.M., Cotterill, C.J., Fielding, J.J., Pearce, R.B. & Croudace, I.W. 2017. A new Holocene record of geomagnetic secular variation from Windermere, UK. *Earth and Planetary Science Letters*, **477**, 108-122.

Baptie, B., Ottemoller, L., Sargeant, S., Ford, G. & O'Mongain, A. 2005. The Dudley earthquake of 2002: A moderate sized earthquake in the UK. *Tectonophysics*, **401**, 1-22.

Barker, P.A., Pates, J., Payne, R. & Healey, R. 2005. Changing nutrient levels in Grasmere, English Lake District, during recent centuries. *Freshwater Biology*, **50**, 1971-1981.

Baskaran, M., Bianchi, T. & Filley, T. 2016. Inconsistencies between ^{14}C and short-lived radionuclides-based sediment accumulation rates: Effects of long-term remineralization. *Journal of Environmental Radioactivity*.

British Geological Survey 2010. UK historical earthquake database. . <http://quakes.bgs.ac.uk/historical/>.

Chaillou, G., Anschutz, P., Dubrulle, C. & Lecroart, P. 2007. Transient states in diagenesis following the deposition of a gravity layer: dynamics of O₂, Mn, Fe and N-species in experimental units. *Aquatic Geochemistry*, **13**, 157-172.

Ciutat, A., Weber, O., Gérino, M. & Boudou, A. 2006. Stratigraphic effects of tubificids in freshwater sediments: a kinetic study based on X-ray images and grain-size analysis. *Acta Oecologica*, **30**, 228-237.

Colley, S., Thomson, J., Wilson, T. & Higgs, N. 1984. Post-depositional migration of elements during diagenesis in brown clay and turbidite sequences in the North East Atlantic. *Geochimica et Cosmochimica Acta*, **48**, 1223-1235.

Croudace, I.W., Rindby, A. & Rothwell, R.G. 2006. ITRAX: description and evaluation of a new multi-function X-ray core scanner. *Geological Society, London, Special Publications*, **267**, 51-63.

Croudace, I.W., Warwick, P.E. & Morris, J.E. 2012. Evidence for the preservation of technogenic tritiated organic compounds in an estuarine sedimentary environment. *Environmental Science & Technology*, **46**, 5704-5712.

Dafoe, L.T., Rygh, A.L., Yang, B., Gingras, M.K. & Pemberton, S.G. 2011. A new technique for assessing tubificid burrowing activities, and recognition of biogenic grading formed by these oligochaetes. *Palaios*, **26**, 66-80.

Davis, R.B. 1974. Stratigraphic effects of tubificids in profundal lake sediments. *Limnol. Oceanogr*, **19**, 466-488.

Davison, W. 1993. Iron and manganese in lakes. *Earth-Science Reviews*, **34**, 119-163.

De Batist, M., Talling, P., Strasser, M. & Girardclos, S. 2017. Subaquatic paleoseismology: records of large Holocene earthquakes in marine and lacustrine sediments. *Marine Geology*, **384**, 1-3.

Dean, J.M., Kemp, A.E.S., Bull, D., Pike, J., Patterson, G. & Zolitschka, B. 1999. Taking varves to bits: Scanning electron microscopy in the study of laminated sediments and varves. *Journal of Paleolimnology*, **22**, 121-136, <http://doi.org/10.1023/a:1008069514445>.

Fisher, J., Lick, W., McCall, P. & Robbins, J. 1980. Vertical mixing of lake sediments by tubificid oligochaetes. *Journal of Geophysical Research: Oceans*, **85**, 3997-4006.

Flynn, W. 1968. The determination of low levels of polonium-210 in environmental materials. *Analytica chimica acta*, **43**, 221-227.

Frouz, J., Lobinske, R.J. & Ali, A. 2004. Influence of Chironomidae (Diptera) faecal pellet accumulation on lake sediment quality and larval abundance of pestiferous midge *Glyptotendipes paripes*. *Hydrobiologia*, **518**, 169-177.

Girardclos, S., Schmidt, O.T., Sturm, M., Ariztegui, D., Pugin, A. & Anselmetti, F.S. 2007. The 1996 AD delta collapse and large turbidite in Lake Brienz. *Marine Geology*, **241**, 137-154.

Gracia, E., Lamarche, G., Nelson, H. & Pantosti, D. 2013. Preface: Marine and Lake Paleoseismology. *Natural Hazards and Earth System Sciences*, **13**, 3469-3478, <http://doi.org/10.5194/nhess-13-3469-2013>.

Hage, S., Hubert-Ferrari, A., Lamair, L., Avşar, U., El Ouahabi, M., Van Daele, M., Boulvain, F., Ali Bahri, M., *et al.* 2017. Flow dynamics at the origin of thin clayey sand lacustrine turbidites: Examples from Lake Hazar, Turkey. *Sedimentology*.

Holmes, P.W. 1964. *Sedimentary studies in Lake Windermere*. University of London.

Howarth, J.D., Fitzsimons, S.J., Norris, R.J. & Jacobsen, G.E. 2012. Lake sediments record cycles of sediment flux driven by large earthquakes on the Alpine fault, New Zealand. *Geology*, **40**, 1091-1094.

Howarth, J.D., Fitzsimons, S.J., Norris, R.J. & Jacobsen, G.E. 2014. Lake sediments record high intensity shaking that provides insight into the location and rupture length of large earthquakes on the Alpine Fault, New Zealand. *Earth and Planetary Science Letters*, **403**, 340-351.

Jarvis, I. & Higgs, N. 1987. Trace-element mobility during early diagenesis in distal turbidites: late Quaternary of the Madeira Abyssal Plain, N Atlantic. *Geological Society, London, Special Publications*, **31**, 179-214.

Kelly, C.A. & Chynoweth, D.P. 1981. The contributions of temperature and of the input of organic matter in controlling rates of sediment methanogenesis. *Limnology and oceanography*, **26**, 891-897.

Kemp, A.E., Pearce, R.B., Pike, J. & Marshall, J.E. 1998. Microfabric and microcompositional studies of Pliocene and Quaternary sapropels from the eastern Mediterranean. *Proceedings of the Ocean Drilling Program Scientific Results*. Ocean Drilling Program, 349-364.

Kemp, A.E.S., Dean, J., Pearce, R.B. & Pike, J. 2001. Recognition and analysis of bedding and sediment fabric features. In: Last, W.M. & Smol, J.P. (eds) *Tracking Environmental Change Using Lake Sediments. Volume 2: Physical and Geochemical Methods*. Kluwer Academic Publishers, Dordrecht, 7-22.

King, G. 1980. A fault plane solution for the Carlisle earthquake, 26 December 1979. *Nature*, **286**, 142-143.

Klaminder, J., Appleby, P., Crook, P. & Renberg, I. 2012. Post-deposition diffusion of ^{137}Cs in lake sediment: Implications for radiocaesium dating. *Sedimentology*, **59**, 2259-2267.

Krinsley, D.H., Pye, K., Boggs Jr, S. & Tovey, N.K. 2005. *Backscattered scanning electron microscopy and image analysis of sediments and sedimentary rocks*. Cambridge University Press.

Lowag, J., Bull, J., Vardy, M., Miller, H. & Pinson, L. 2012. High-resolution seismic imaging of a Younger Dryas and Holocene mass movement complex in glacial lake Windermere, UK. *Geomorphology*, **171**, 42-57.

McCall, P.L. & Tevesz, M.J. 1982. The effects of benthos on physical properties of freshwater sediments *Animal-Sediment Relations*. Springer, 105-176.

McGowan, S., Barker, P., Haworth, E.Y., Leavitt, P.R., Maberly, S.C. & Pates, J. 2012. Humans and climate as drivers of algal community change in Windermere since 1850. *Freshwater Biology*, **57**, 260-277.

Miller, H., Cotterill, C.J. & Bradwell, T. 2014. Glacial and paraglacial history of the Troutbeck Valley, Cumbria, UK: integrating airborne LiDAR, multibeam bathymetry, and geological field mapping. *Proceedings of the Geologists' Association*, **125**, 31-40.

Miller, H., Bull, J.M., Cotterill, C.J., Dix, J.K., Winfield, I.J., Kemp, A.E. & Pearce, R.B. 2013. Lake bed geomorphology and sedimentary processes in glacial lake Windermere, UK. *Journal of Maps*, **9**, 299-312.

Moernaut, J., De Batist, M., Heirman, K., Van Daele, M., Pino, M., Brümmer, R. & Urrutia, R. 2009. Fluidization of buried mass-wasting deposits in lake sediments and its relevance for paleoseismology: results from a reflection seismic study of lakes Villarrica and Calafquén (South-Central Chile). *Sedimentary Geology*, **213**, 121-135.

Moernaut, J., Daele, M.V., Heirman, K., Fontijn, K., Strasser, M., Pino, M., Urrutia, R. & De Batist, M. 2014. Lacustrine turbidites as a tool for quantitative earthquake reconstruction: New evidence for a variable rupture mode in south central Chile. *Journal of Geophysical Research: Solid Earth*, **119**, 1607-1633.

Monecke, K., Anselmetti, F.S., Becker, A., Sturm, M. & Giardini, D. 2004. The record of historic earthquakes in lake sediments of Central Switzerland. *Tectonophysics*, **394**, 21-40.

Musson, R. 1998. The Barrow-in-Furness earthquake of 15 February 1865: liquefaction from a very small magnitude event. *pure and applied geophysics*, **152**, 733-745.

Musson, R. & Henni, P. 2002. The felt effects of the Carlisle earthquake of 26 December 1979. *Scottish Journal of Geology*, **38**, 113-125.

Musson, R. & Sargeant, S. 2007. Eurocode 8 seismic hazard zoning maps for the UK. *Nottingham, UK, British Geological Survey*, **CR/07/125N**, 62.

Nisbet, E.G. & Piper, D.J. 1998. Giant submarine landslides. *Nature*, **392**, 329-330.

Nogaro, G., Mermillod-Blondin, F., Montuelle, B., Boisson, J.-C. & Gibert, J. 2008. Chironomid larvae stimulate biogeochemical and microbial processes in a riverbed covered with fine sediment. *Aquatic Sciences-Research Across Boundaries*, **70**, 156-168.

Olafsson, J. 1992. Vertical microdistribution of benthic chironomid larvae within a section of the littoral zone of a lake. *Netherland Journal of Aquatic Ecology*, **26**, 397-403.

Pickering, A.D. & Sutcliffe, D. 2001. *Windermere: restoring the health of England's largest lake*. Freshwater Biological Association.

Pinson, L.J., Vardy, M.E., Dix, J.K., Henstock, T.J., Bull, J.M. & Maclachlan, S.E. 2013. Deglacial history of glacial lake Windermere, UK: implications for the central British and Irish Ice Sheet. *Journal of Quaternary Science*, **28**, 83-94.

Reynoldson, T.B. 1987. The role of environmental factors in the ecology of tubificid oligochaetes-an experimental study. *Ecography*, **10**, 241-248.

Ritchie, J.C. & McHenry, J.R. 1990. Application of radioactive fallout cesium-137 for measuring soil erosion and sediment accumulation rates and patterns: a review. *Journal of environmental quality*, **19**, 215-233.

Robbins, J.A. 1978. Geochemical and geophysical applications of radioactive lead isotopes. In: Nriagu, J.O. (ed) *Biochemistry of Lead*. Elsevier, Amsterdam, 285-393.

Sabater, S. & Haworth, E.Y. 1995. An assessment of recent trophic changes in Windermere South Basin (England) based on diatom remains and fossil pigments. *Journal of Paleolimnology*, **14**, 151-163.

Schimmelmann, A., Lange, C.B., Schieber, J., Francus, P., Ojala, A.E.K. & Zolitschka, B. 2016. Varves in marine sediments: A review. *Earth-Science Reviews*, **159**, 215-246, <http://doi.org/10.1016/j.earscirev.2016.04.009>.

Schlolaut, G., Brauer, A., Marshall, M.H., Nakagawa, T., Staff, R.A., Ramsey, C.B., Lamb, H.F., Bryant, C.L., *et al.* 2014. Event layers in the Japanese Lake Suigetsu 'SG06' sediment core: Description, interpretation and climatic implications. *Quaternary Science Reviews*, **83**, 157-170.

Simonneau, A., Chapron, E., Vanniere, B., Wirth, S., Gilli, A., Di-Giovanni, C., Anselmetti, F., Desmet, M., *et al.* 2013. Mass-movement and flood-induced deposits in Lake Ledro, southern Alps, Italy: implications for Holocene palaeohydrology and natural hazards. *Climate of the Past*, **9**, 825-840.

Strasser, M., Monecke, K., Schnellmann, M. & Anselmetti, F.S. 2013. Lake sediments as natural seismographs: A compiled record of Late Quaternary earthquakes in Central Switzerland and its implication for Alpine deformation. *Sedimentology*, **60**, 319-341, <http://doi.org/10.1111/sed.12003>.

Stucchi, M., Rovida, A., Capera, A.G., Alexandre, P., Camelbeeck, T., Demircioglu, M., Gasperini, P., Kouskouna, V., *et al.* 2013. The SHARE European earthquake catalogue (SHEEC) 1000–1899. *Journal of Seismology*, **17**, 523-544.

Thomson, J., Colley, S., Higgs, N., Hydes, D., Wilson, T. & Sørensen, J. 1987. Geochemical oxidation fronts in NE Atlantic distal turbidites and their effects in the sedimentary record. *Geological Society, London, Special Publications*, **31**, 167-177.

Tylmann, W., Bonk, A., Goslar, T., Wulf, S. & Grosjean, M. 2016. Calibrating Pb-210 dating results with varve chronology and independent chronostratigraphic markers: Problems and

implications. *Quaternary Geochronology*, **32**, 1-10,
<http://doi.org/10.1016/j.quageo.2015.11.004>.

Van Daele, M., Moernaut, J., Silversmit, G., Schmidt, S., Fontijn, K., Heirman, K., Vandoorne, W., De Clercq, M., *et al.* 2014. The 600 yr eruptive history of Villarrica Volcano (Chile) revealed by annually laminated lake sediments. *Geological Society of America Bulletin*, **126**, 481-498.

Van Daele, M., Moernaut, J., Doom, L., Boes, E., Fontijn, K., Heirman, K., Vandoorne, W., Hebbeln, D., *et al.* 2015. A comparison of the sedimentary records of the 1960 and 2010 great Chilean earthquakes in 17 lakes: Implications for quantitative lacustrine palaeoseismology. *Sedimentology*, **62**, 1466-1496.

Vardy, M.E., Pinson, L.J., Bull, J.M., Dix, J.K., Henstock, T.J., Davis, J.W. & Gutowski, M. 2010. 3D seismic imaging of buried Younger Dryas mass movement flows: Lake Windermere, UK. *Geomorphology*, **118**, 176-187.

Wilhelm, B., Nomade, J., Crouzet, C., Litty, C., Sabatier, P., Belle, S., Rolland, Y., Revel, M., *et al.* 2016. Quantified sensitivity of small lake sediments to record historic earthquakes: implications for paleoseismology. *Journal of Geophysical Research: Earth Surface*, **121**, 2-16.

Zolitschka, B., Francus, P., Ojala, A.E.K. & Schimmelfmann, A. 2015. Varves in lake sediments - a review. *Quaternary Science Reviews*, **117**, 1-41.

Figure captions

Fig. 1 Map of sample locations: Map of the Windermere catchment with 200 m contour lines, multibeam lake bathymetry, and sediment sample locations. Thick black line represent catchment boundaries of 1: Esthwaite Water, 2: Brathay River, 3: Rothay River and 4: Troutbeck. Inset: Location of Windermere in the British Isles (black box), and Carlisle Earthquake epicentre (black star).

Fig. 2 Trout Beck debris flow; (a) hillshade bathymetry (x5 vertically exaggerated), (b) bathymetric map of Trout Beck debris flow showing position of core 53 and a grab sample within the scarp and location of bottom photograph of (c). (c) Photograph of exposed laminated glacial clay (taken with remotely operated vehicle) within the sidewall of the Troutbeck debris flow scarp. (d) Photograph of grab sample showing 7 cm of Holocene mud unconformably overlying laminated clays. The unconformity represents the debris flow failure plane. The top surface of the grab sample is the lakebed surface, indicating no mud was lost during collection of the sample.

Fig. 3. Overall stratigraphy for SC68, SC64, SC67 and SC57. Core depth in cm, core photograph, core x-radiograph, lithostratigraphy and ED-XRF K for all four gravity cores collected from Windermere. Water depth of each coring site is shown above the corresponding core. The grey lines shows correlation between the clay facies (mass transport deposit) in the North Basin cores and contemporary facies boundary in the South Basin cores demonstrating the absence of the pale clay horizon from the South Basin.

Fig. 4. Measurements of artificial radionuclides for cores SC64 (a) and SC68 (b) with vertical error indicates bulk sample interval and horizontal error represents the machine measurement error, the red circle in 4b shows outlying data removed from analysis. Also shown is $\text{Ln } ^{210}\text{Pb}$ used to calculate mean sedimentation rates (MSR) where R^2 shows the linear trend for the $\text{Ln } ^{210}\text{Pb}$ data. Right shows the age depth model with black circles showing the ^{210}Pb CF:CS MSR age depth model at 10 cm intervals. Vertical error indicates bulk sample interval and horizontal error represents the extent of the maximum and minimum age depth based on machine measurement error. Grey circles show the ^{137}Cs based age depth at 1986 with vertical error also indicating the bulk sample interval.

Fig. 5 North Basin cores (a) SC64; (b) SC68 are shown with core depth (cm), core photograph, core x-radiograph and stratigraphy (and legend bottom right of the figure), together with Mn itrax values for the core. Dashed black lines show the position of the Back Scatter Electron Image (BSEI) within the cores. BSEI are shown with depth (cm) and K, and Ti, ED-XRF geochemistry (element counts/ total kcps) for the BSEI interval is plotted by the black lines, and WD-XRF (%) are plotted as red dots with the error bars representing the sampling interval. Black arrows right of the BSEI show the location of the clay horizon in SC64 (c) and in SC68 (e), and more detail of bioturbation and pellets in SC68 (d).

Fig. 6 SC68 mass transport deposit (MTD) back scatter electron image, sediment fabric types, K ED line scan 5 point running average (black dots) and raw counts (grey line) with clay redistribution zone highlighted. The figure highlights the extent to which the MTD has been vertically redistributed from the original clay deposit (dotted line).

Fig. 7 Core photograph and stratigraphy of core 53 taken from within the Trout Beck mass transport deposit (MTD). The MTD is highlighted in grey, unconformably overlying laminated clays.

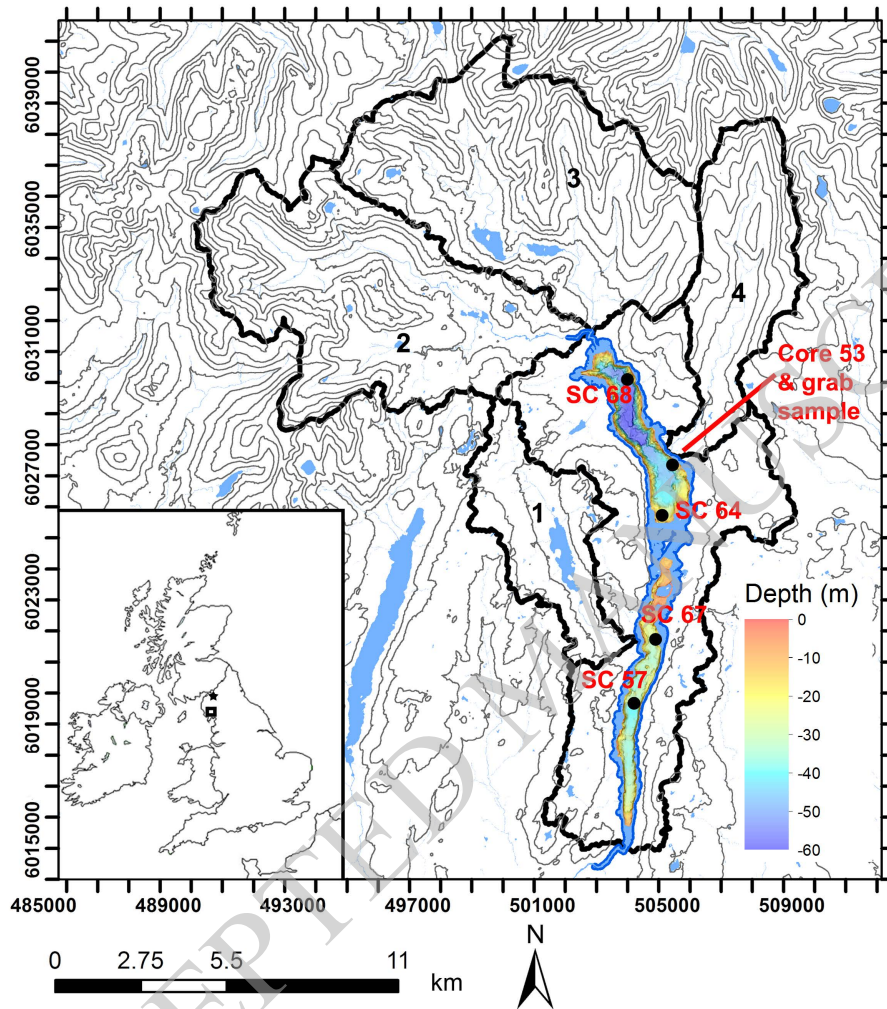
Fig. 8 Black line shows river discharge data for the River Levin from 1939 – 2014. The black dot shows the timing of the mass transport deposit (MTD) in SC68 and the white dot the timing of the MTD in SC64. Error bars on both show the machine error derived age range.

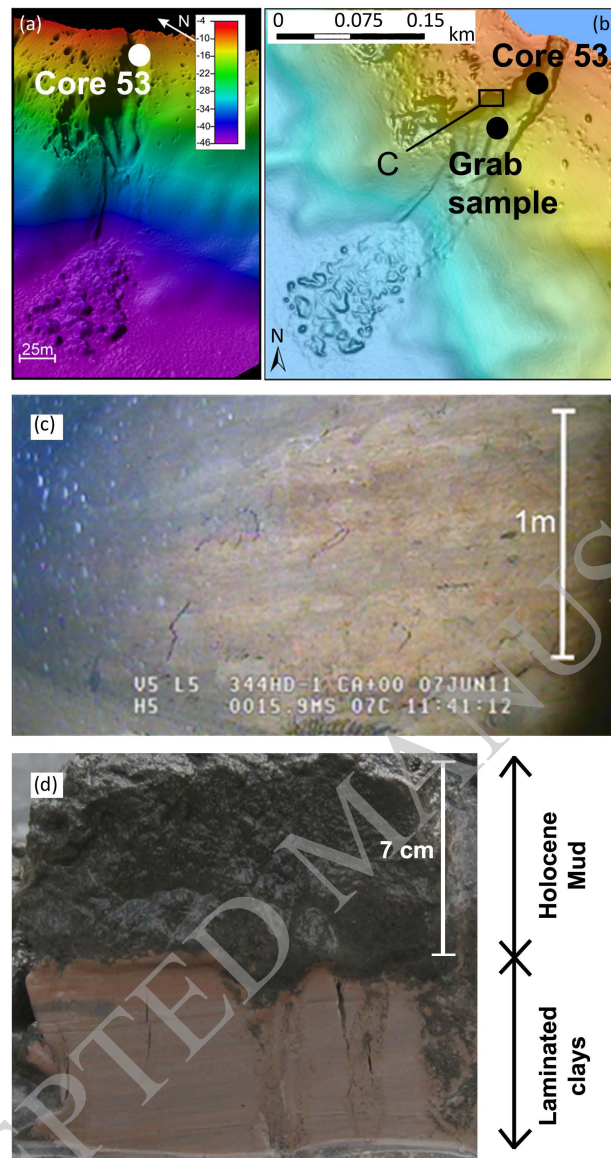
Fig. 9 An illustration of the processes that generate the clay horizon in the North Basin of Windermere. (a) Trout Beck debris flow is triggered which removes Holocene mud from the

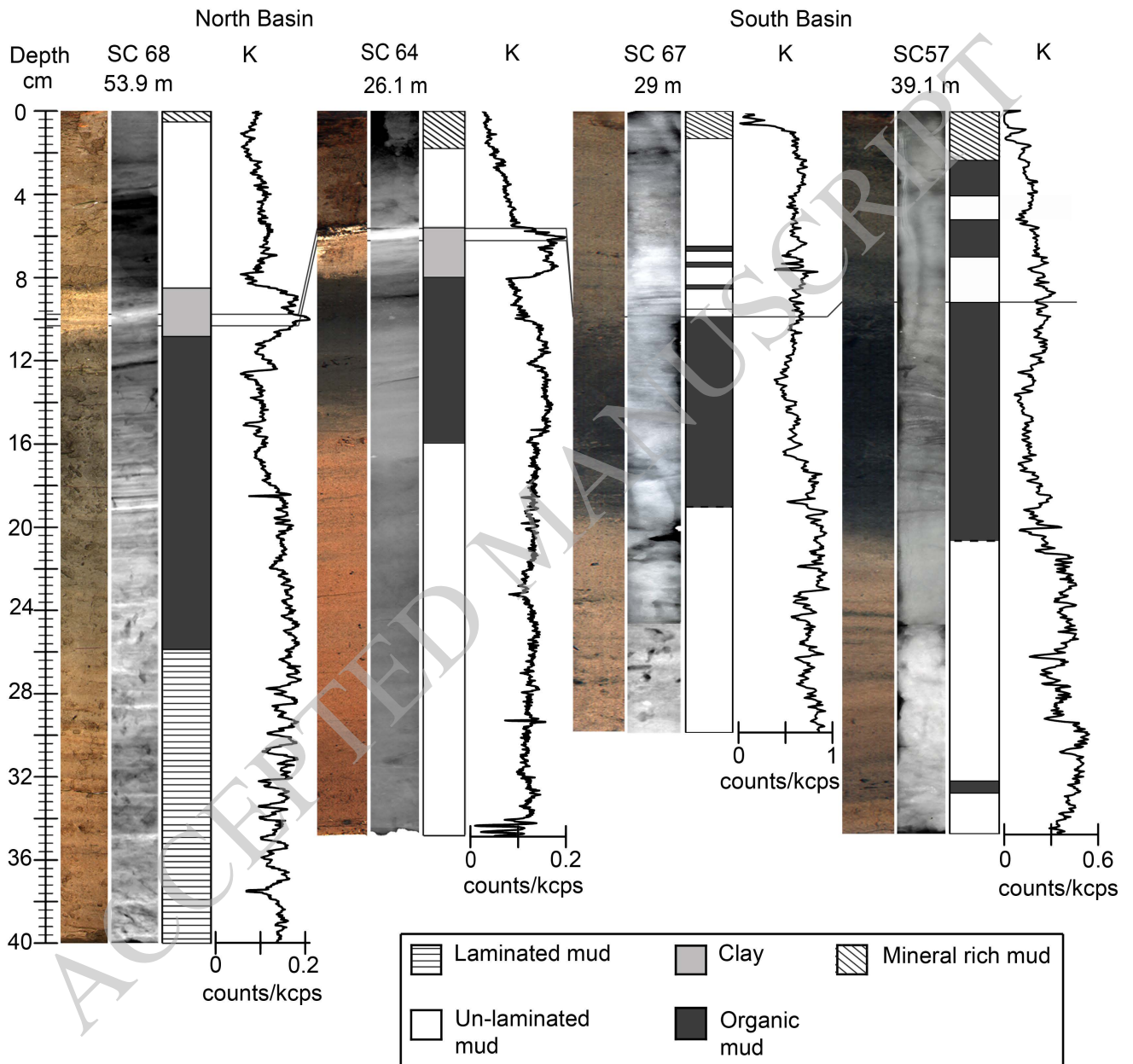
slope and deposits it as a debris flow. The scarp failure exposes the pre-Holocene clays within the scarp. **(b)** Fine particle matter suspended in the water column below the level of the scarp settle over the North Basin of Windermere. Within the scarp small scale mass transport deposits further redistribute sediment (see Fig. 7). **(c)** Mud continues to deposit on top of the clay horizon. **(d)** Mn – Fe lamination formation in deep anoxic and shallow oxic settings. On the left a schematic of SC68 shows Mn and Fe in solution being removed from the sediment pore water to the water column above in an anoxic bottom water environment. The right shows a schematic of SC64 with ventilated bottom water and a redox boundary within the sediment at which the reductively mobilised Mn and Fe are precipitated as oxyhydroxides above the MTD.

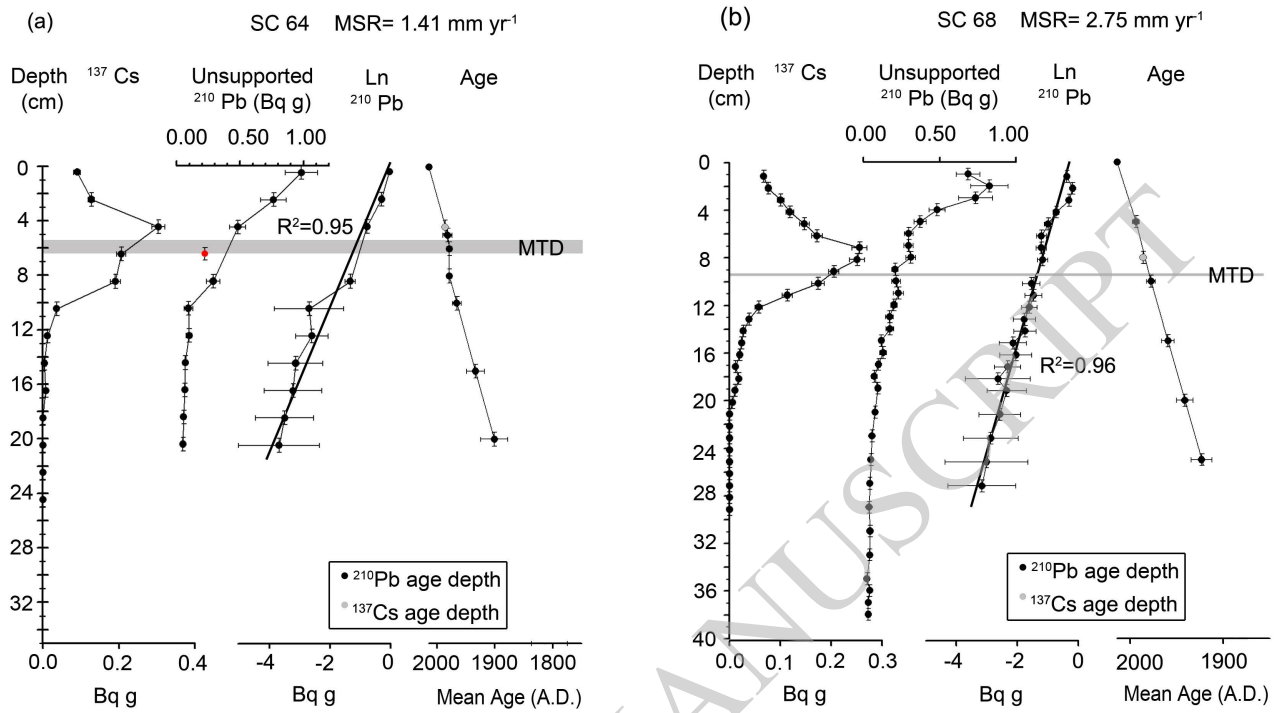
Table 1: Results of XRD desecrate samples from SC64 debris lamina, Plag=plagioclase feldspar, Qtz=quartz, Chl=chlorite, Musc=muscovite mica.

XRD: SC64 debris lamina sample						
Normalised total	Mineralogy					
			Clays		Total Clay	
	Plag	Qtz	Chl	Musc	(Chl+Musc)	TOTAL
	14.6%	52.8%	7.2%	25.4%	32.6%	100.0%
Absolute total	Mineralogy					
			Clays		Total Clay	
	Plag	Qtz	Chl	Musc	(Chl+Musc)	TOTAL
	13.3%	48.3%	6.6%	23.2%	32.6%	91.4%

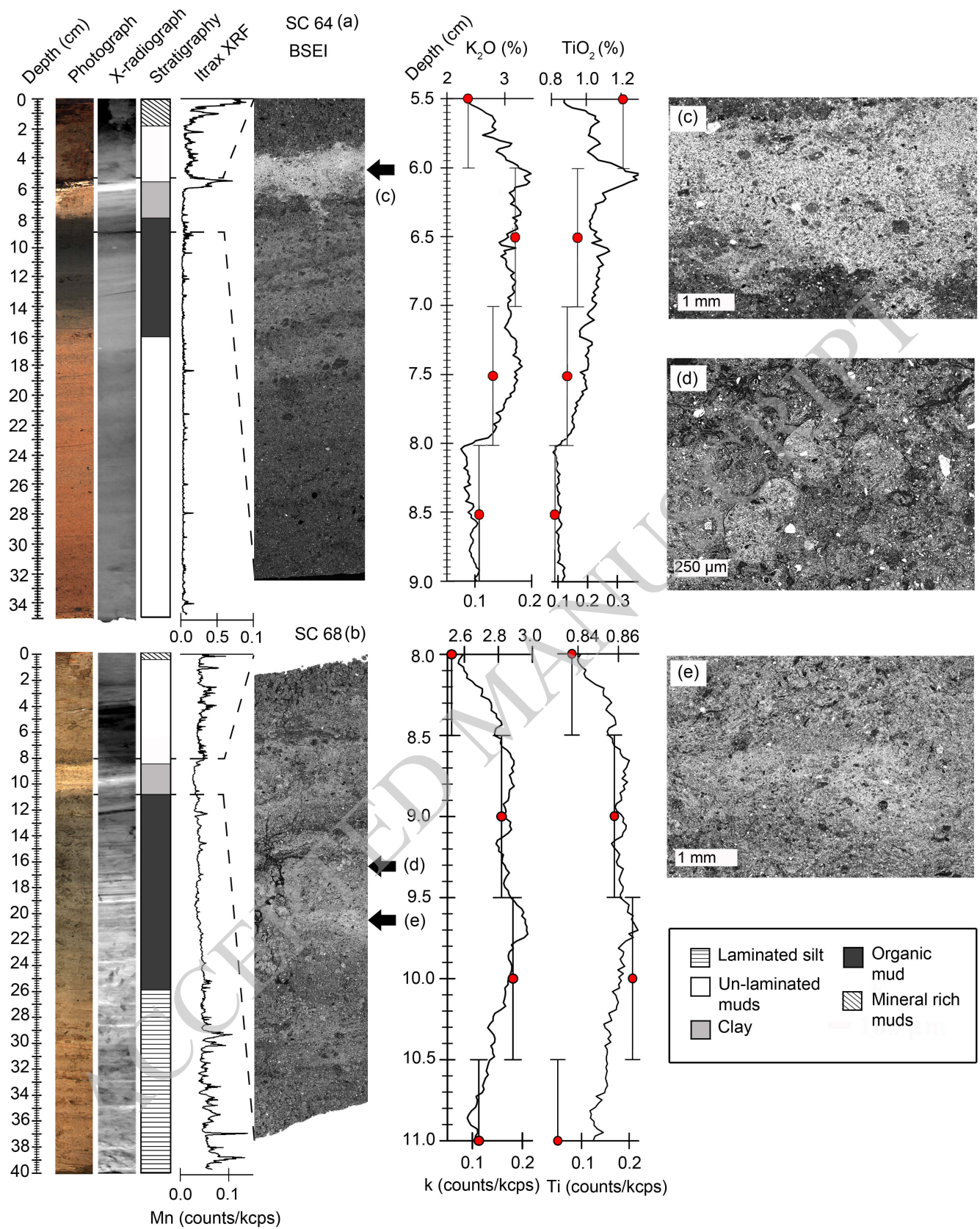


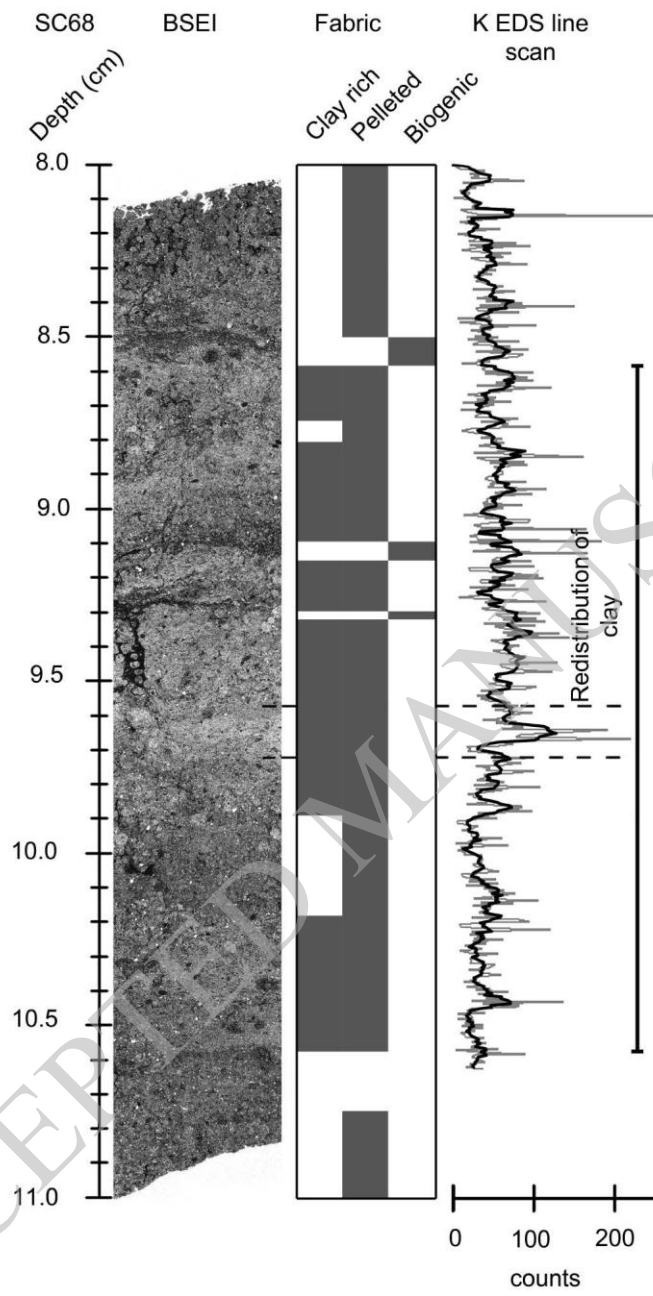


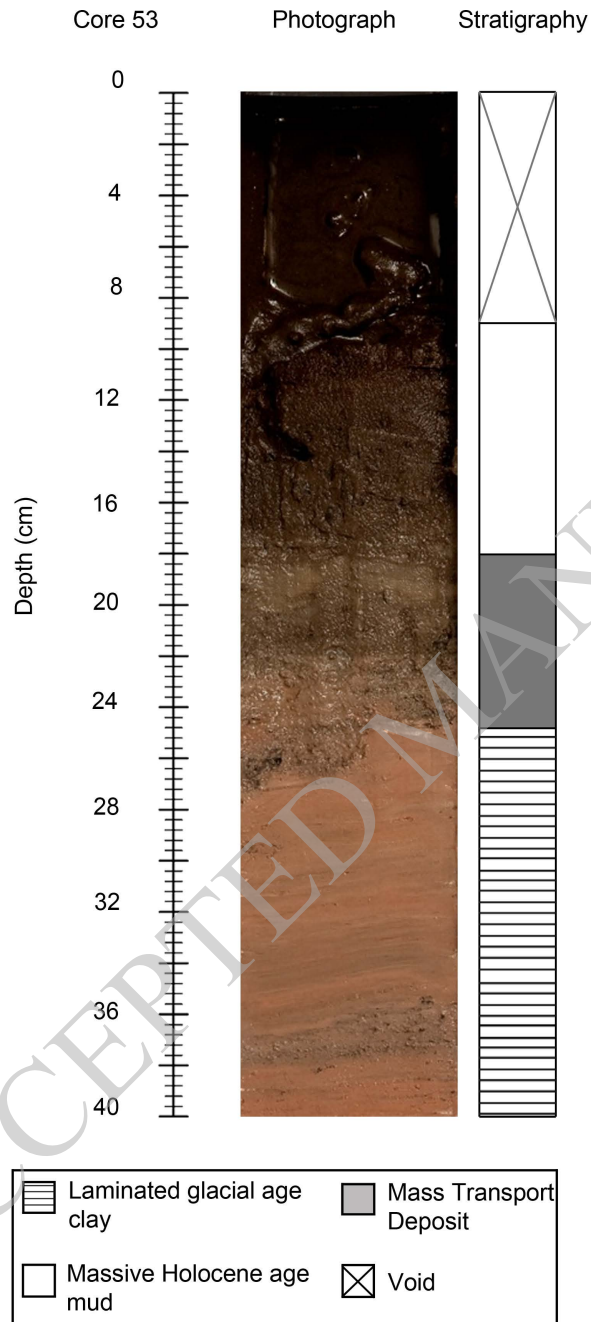


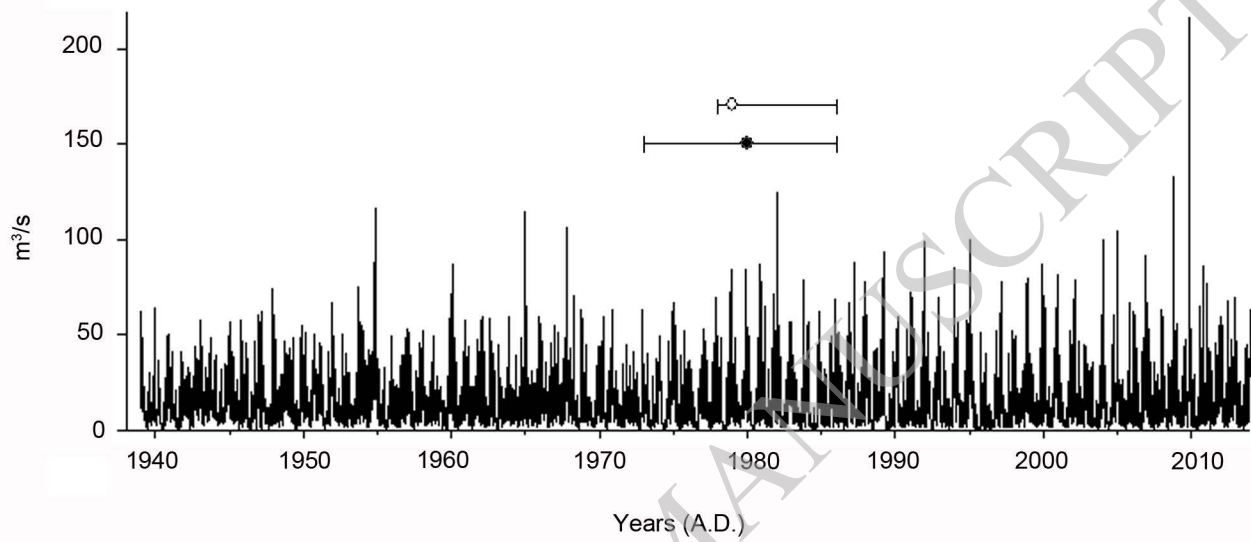


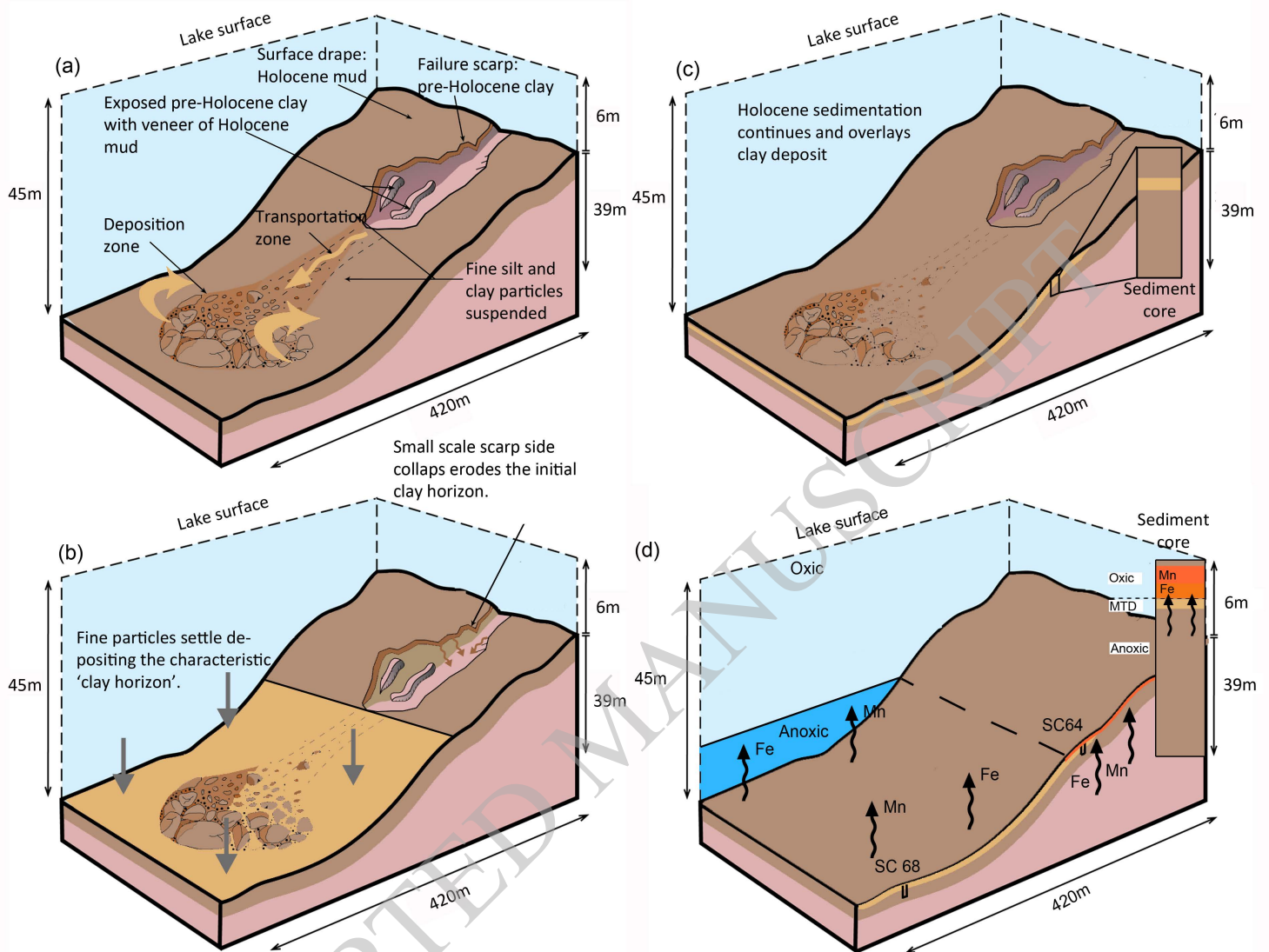
ACCEPTED MANUSCRIPT











ACCEPTED MANUSCRIPT